

R. K. Ellis  
Fermi National Accelerator Laboratory, Batavia, IL 60510

Summary

Using the example of vector boson production, the application of the QCD improved parton model at collider energies is reviewed. The reliability of the extrapolation to SSC energies is assessed. Predictions at  $\sqrt{s} = 0.54$  TeV are compared with data.

Predictions for the interactions of hadrons in the TeV range are usually made using the parton model, suitably modified to include the effects due to QCD. The model has been remarkably successful in analysis of experiments at fixed target energies, but present colliders test the model in a new energy regime, which will be further extended by the projected super colliders. This extension of the kinematic range raises certain theoretical issues which are addressed here, and elsewhere in these proceedings. It is also of interest to compare the predictions of the model with data at  $\sqrt{s} = 0.54$  TeV, in order to assess the accuracy of projections to super-collider energies. This program is carried out in this paper.

Schematically, the parton model cross-section may be written as

$$\sigma(P_i) = \sum_{j,k} \int dx_1 dx_2 f_j(x_1, Q^2) f_k(x_2, Q^2) \sigma_{jk}(x_1) \quad (1)$$

where  $f_j$  are the parton distributions and  $j, k$  run over parton species. The QCD parton model contains three ingredients. These are,

- a) the specification of distributions of quarks, antiquarks and gluons inside the colliding hadrons.
- b) the extrapolation of the parton distributions to the higher energies relevant for collider experiments.
- c) the calculations of parton cross-sections which, when combined with the parton distributions, fix the overall hadronic cross-section.

The first topic, the measurement of the parton densities will only be mentioned briefly. The principal source of information on these distributions comes from deep-inelastic lepton hadron scattering. For a review of the experimental problems in these determinations we refer the reader to ref.(3). The shape of the valence quark distributions is well determined. The uncertainties in the measurement of the antiquark distributions are somewhat larger, but the distributions themselves are smaller at fixed target energies. The shape of the gluon distribution, which is determined from scaling violations in deep-inelastic scattering, is correlated with the measured value of the scale breaking parameter  $\Lambda$ .

Setting aside the question of the experimental determination of the parton distributions, we now discuss the extrapolation to collider energies. In general the parton distribution functions are required at values of  $x$  and  $Q^2$  which are outside the range measured in deep-inelastic scattering. The particular values depend on the transverse energy or mass of the object being produced. A W-boson produced in proton anti-proton collisions at  $\sqrt{s} = 0.54$  TeV is most likely to have come from a pair of partons having a fraction

$x = 0.15$  of the hadrons' longitudinal momentum. Values of  $x$  which are higher or lower are probed if the W is produced in the forward or backward direction. At  $\sqrt{s} = 40$  TeV the typical value of  $x$  has become  $x = 2.0 \times 10^{-3}$ , although in the measurable rapidity range, one is sensitive to values as small as  $x = 10^{-4}$ . For the production of hypothetical heavier particles, say of mass  $Q$ , the values of  $x$  are larger but the values of  $Q^2$ , at which the distribution is needed are also larger. We are therefore interested in a range such that,

$$Q/x < E \quad (2)$$

where  $E$  is the total centre of mass energy of the collider.

The extrapolation to the values of  $x$  and  $Q^2$  required is performed using the Altarelli-Parisi equation.

$$\frac{d}{d(\ln Q^2)} \begin{pmatrix} q(x) \\ G(x) \end{pmatrix} = \frac{\alpha_s(Q^2)}{2\pi} \int_x^1 \frac{dz}{z} \begin{pmatrix} P_{qq}(z) & P_{qG}(z) \\ P_{Gq}(z) & P_{GG}(z) \end{pmatrix} \begin{pmatrix} q(\frac{x}{z}) \\ G(\frac{x}{z}) \end{pmatrix} \quad (3)$$

The functions  $P$  are the evolution kernels which are calculated as a perturbation series in the strong coupling constant. Normally the equations are used including only the first order evolution kernel, although the second order terms and certain terms of even higher orders have also been calculated. As the evolution proceeds uncertainties in the sea and gluon distribution functions tend to diminish. This is shown in Fig. (1) for the case of the gluon distribution function at  $Q^2 = 4 \text{ GeV}^2$  and  $Q^2 = 2000 \text{ GeV}^2$ . The curves which are very different at low  $Q^2$  approach one another at high  $Q^2$ . These curves were obtained using the two parameterisations of Duke and Owens which evolve with different values of  $\Lambda$ . Part of the reason why different starting distributions, (compatible with data), give similar results after evolution is that Eq. (3) is driven by the hardest term on the right hand side, which is the well measured valence distribution.

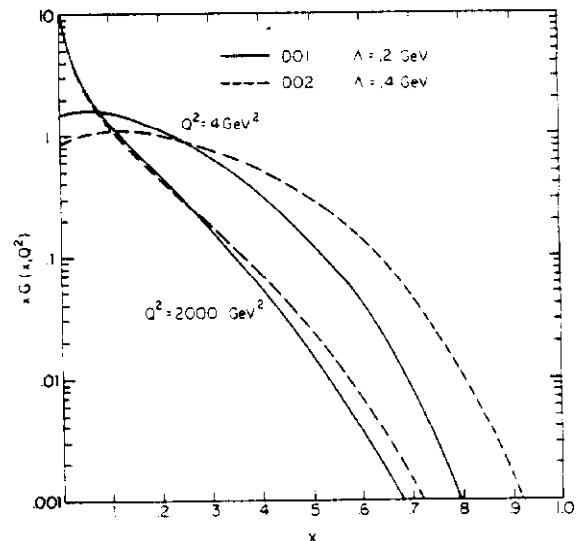


Fig. 1  
Two parameterisations for the gluon distribution function at  $Q^2 = 4 \text{ GeV}^2$  and  $Q^2 = 2,000 \text{ GeV}^2$ .

The extrapolation using the first-order Altarelli-Parisi kernels is expected to be acceptable throughout the range explored at super-collider energies. A possible source of danger is the low x region, untested by fixed target experiments. As already mentioned above, despite our ignorance of these distributions at low x and  $Q^2$ , the AP equations are expected to give a reliable estimate at low x and higher  $Q^2$ . This is because the growth at low x, due to parton cascade from higher x, is so much larger than the presumed starting value at low x. The issue is whether the AP equations with first order kernels are an accurate representation of the behaviour of the theory in this region. The one loop evolution equations at low x are dominated by the poles at  $x = 0$  which appear in the splitting functions. In the limit  $x \rightarrow 0, (C_A=3, C_F=4/3),$

$$P_{GG}^{(1)}(x) = \frac{\alpha_s}{2\pi} \frac{2C_A}{x} ; P_{Gq}^{(1)} = \frac{\alpha_s}{2\pi} \frac{2C_F}{x} \quad (4)$$

In this approximation, the gluon distribution function evolves according to

$$\frac{dG(x, Q^2)}{d \ln Q^2} = \frac{C_A}{x} \frac{\alpha_s(Q^2)}{\pi} \int_x^1 dz G(z, Q^2) \quad (5)$$

The solution to this equation in the limit in which  $\ln(1/x) \ln(\ln Q^2) \gg 1$  is,

$$G(x, Q^2) = \frac{1}{x} \exp \sqrt{\frac{4C_A}{\pi b} \ln \left( \frac{\ln Q^2}{A^2} \right) \ln \frac{1}{x}} \quad (6)$$

where  $[b\alpha_s(Q^2)]^{-1} = \ln Q^2/A^2$ . The second order splitting function does not lead to a large modification of this behaviour; at small x the matrix of evolution kernels is given by,

$$xP^{(2)} = \left( \frac{\alpha_s}{2\pi} \right)^2 \begin{pmatrix} \frac{40}{9} C_F T_R n_f & \frac{40}{9} C_A T_R n_f \\ C_F C_A - \frac{40}{9} C_F T_R n_f & \frac{4}{3} (C_F \frac{C_A}{2}) - \frac{40}{9} C_A T_R n_f \end{pmatrix} \quad (7)$$

This equation should be compared with the corresponding results for the timelike case. For example, the function which controls the fragmentation of a gluon is given by,

$$P_{GG}^T \underset{x \rightarrow 0}{=} \frac{\alpha_s}{2\pi} \frac{2C_A}{x} - \left( \frac{\alpha_s}{2\pi} \right)^2 \frac{4C_A^2 \ln^2 x}{x} + \dots \quad (8)$$

and after resummation to all orders the moments of this function are known to be given by,

$$Y_{GG}^T(n) = \frac{1}{4} \left[ -(n-1) + \sqrt{(n-1)^2 + \frac{8\alpha_s C_A}{\pi}} \right] \quad (9)$$

Returning to the spacelike case we see from Eq. (7) that terms of order  $\alpha_s^2 \ln(1/x)^m/x$  for  $m=1,2$  are absent. Indeed it is known that to all orders the most singular terms in the perturbation series for the splitting function are of the form,

$$P_{GG}(x) = \sum_{j=0}^{\infty} a_j \frac{\kappa}{x} (\kappa \ln \frac{1}{x})^j ; \kappa = \left( \frac{\alpha_s C_A}{\pi} \right) \quad (10)$$

The values of the coefficients  $a_j$  are known.<sup>6</sup> Note that  $a_1 = a_2 = 0$ . Since the correction terms are of order  $\kappa \ln(1/x)$ , we should not envisage any problems with perturbation theory until  $\kappa \ln(1/x) \approx 1$ . Thus the first order equations provide an adequate description at least down to values,

$$x > 10^{-3} \text{ at } Q^2 = 10^4 \text{ GeV} \quad (11)$$

In ref. (2) it is argued that lowest order perturbation theory should be valid to even smaller values of x, because of the steepness near  $x = 0$ , with which the splitting function is convoluted. However, Eq. (11) is sufficient for most purposes at energies  $E < 40 \text{ TeV}$ .

In order to make numerical estimates of the cross-sections we will use the results of numerical integration of the Altarelli-Parisi equation given in the literature. The parameterisations which we consider are those of Duke and Owens (DO),<sup>7</sup> Gluck Hoffmann and Reya (GHR)<sup>11</sup> and Eichten, Hinchliffe, Lane and Quigg (EHLQ).<sup>12</sup> None of the parameterisations is entirely satisfactory throughout the range  $\sqrt{s}=0.5-40 \text{ TeV}$ . A satisfactory parameterisation must a) be compatible with the data at fixed target energies, b) give a satisfactory fit to the result of numerical evolution of the low energy distributions throughout the range of collider and super-collider energies (cf. eq.(11)). The stated range of accuracy of the three sets is

$$\begin{aligned} \text{DO: } & 5 \cdot 10^{-3} < x < 1 \quad 2 < Q < 10^3 \text{ GeV (few \%)} \\ \text{GHR: } & 10^{-2} < x < 1 \quad 2 < Q < 200 \text{ GeV} \\ \text{EHLQ: } & 10^{-4} < x < 1 \quad 2.3 < Q < 10^4 \text{ GeV (5\%)} \end{aligned} \quad (12)$$

where the percentage is the estimated maximum deviation of the parameterisation from the result of the numerical evolution of the starting distributions. Thus we see that the first two sets have an x range somewhat less than desired for super-collider energies.

Not all features of fixed target data are reproduced by the parameterisations, although there is some degree of choice in the data sets which are used. The DO parameterisations have an SU(3) symmetric sea which appears to be excluded by the data.<sup>5</sup> Since sea distributions are important at super-collider energies, this deficiency can lead to noticeable differences. The ratio of valence down and up quarks is measured to be approximately given by

$$d_V(x)/u_V(x) = 0.57(1-x) \quad (13)$$

The EHLQ structure functions fit this ratio rather poorly (see ref.(12)) and hence somewhat underestimate W production cross-sections at CERN collider energies. Different theoretical treatments of the charm quark threshold can lead to appreciable differences at small values of x. Generally speaking these incompatibilities of the parton distribution functions with data lead to less than 20% effects in the final cross-sections, nevertheless they introduce an avoidable source of error.

The total cross-sections for vector boson production in pp collisions at CERN collider energies including the  $O(\alpha_s)$  corrections have been presented in ref. (13). The gluonic radiative corrections were implemented following the basic strategy of ref. (14). Inclusion of the  $O(\alpha_s)$  corrections increases the zero order cross-section - the so-called K factor - by about 30%. This is to be compared with the  $O(\alpha_s)$  correction in Drell-Yan production at fixed target energies which is about 80%. This decrease in the size of the radiative correction is mainly due to the decrease in the size of the running coupling  $\alpha_s$ . The contribution of the initial gluons after factorisation is negative and less than a 5% correction.

The theoretical calculations of the cross-sections for pp collisions at  $\sqrt{s} = 0.54$  TeV are,

$$\sigma_{W^+W^-} = (4.2 \pm 1.3)_{-0.6} \text{ nb} ; \quad \sigma_{Z^0} = (1.3 \pm 0.4)_{-0.2} \text{ nb} \quad (14)$$

The theoretical uncertainties in these cross-sections have been estimated by using different sets of parton distributions and different arguments for the running coupling. The value for the W cross-section found using the EHLQ structure function is somewhat low but lies within the range given in Eq. (14). The ratio of the two cross-sections, important for counting neutrinos is less subject to theoretical error,

$$\frac{\sigma_{W^+ + W^-}}{\sigma_{Z^0}} = 3.3 \pm 0.2 \quad (15)$$

Multiplying Eqs. (14) by the branching ratio into electrons,

$$B(W \rightarrow e\nu) = 0.089 \quad B(Z^0 \rightarrow e^+e^-) = 0.032 \quad (16)$$

which are the values obtained for a top quark mass  $m_t = 40$  GeV and  $\alpha_s/\pi = 0.04$ , we find that the product of the cross-section and decay branching ratio is,

$$(\sigma_B)_{W^\pm \rightarrow e^\pm} = (370 \pm 110)_{-60} \text{ pb}$$

$$(\sigma_B)_{Z^0 \rightarrow e^+e^-} = (42 \pm 12)_{-6} \text{ pb} \quad (17)$$

The corresponding experimental results are<sup>15,16</sup>

$$\text{UA1} : (\sigma_B)_{W^\pm} = 530 \pm 80 \pm 90 \text{ pb} \quad (\sigma_B)_{Z^0} = 71 \pm 24 \pm 13 \text{ pb} \quad (18)$$

$$\text{UA2} : (\sigma_B)_{W^\pm} = 530 \pm 100 \pm 100 \text{ pb} \quad (\sigma_B)_{Z^0} = 110 \pm 40 \pm 20 \text{ pb} \quad (19)$$

Theoretical predictions for higher energies are given in Table (1). These results are also subject to theoretical error. Fig. (2) displays these results for a fixed set of parton distribution functions (Duke and Owens', Set 1) and a given choice of scale for  $\alpha_s(Q=M_W)$ . The solid curve is for proton-antiproton and the dotted curve is for proton-proton collisions. Above  $\sqrt{s} = 10$  TeV the two curves are essentially identical because of the dominance of sea quarks. Also shown plotted are the cross-sections for the production of hypothetical bosons of mass 0.2, 0.5 and 1 TeV which couple to quarks exactly in the same way as the normal W boson. These curves are also subject to theoretical uncertainties similar to those in Table 1. Although the cross-section for the production of W bosons at 40 TeV is large, it should be borne in mind that only about 30% of them occur at observable rapidities  $y < 2$ . A W produced at rapidity greater than 2 lies within  $15^\circ$  of the beam pipe.

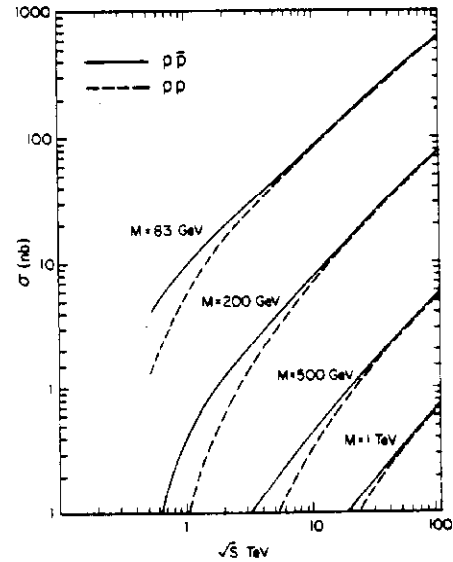


Fig. 2  
The total cross-section for the production of  $W^+W^-$  bosons,  $M = 83$  GeV in proton antiproton collisions (solid line) and proton proton collisions (dashed line). The other curves refer to heavier charged bosons with the same couplings to quarks as the W of the standard model.

$\sqrt{s}$ (TeV)	$\sigma_{W^+W^-} (M_W=83 \text{ GeV})$ (nb)	$\sigma_{Z^0} (M_Z=94 \text{ GeV})$ (nb)
0.54	$4.2^{+1.3}_{-0.6}$	$1.3^{+0.4}_{-0.2}$
0.63	$5.3^{+1.6}_{-0.9}$	$1.6^{+0.5}_{-0.3}$
1.6	$16.0^{+4.0}_{-2.5}$	$4.9^{+1.2}_{-0.8}$
2.	$20. \quad ^{+6.}_{-4.}$	$6.2^{+1.9}_{-1.2}$
10.	$75. \quad ^{+35.}_{-25.}$	$27. \quad ^{+12.}_{-9.}$
20.	$130. \quad ^{+70.}_{-55.}$	$46. \quad ^{+24.}_{-20.}$
40.	$190. \pm 100.$	$70. \pm 30.$

Table 1  
Theoretical results for the W and Z total cross-sections in pp interactions at various energies. Estimates of the theoretical error are also given.

We now consider the transverse momentum of the produced vector bosons in more detail. This is a subject of both theoretical and practical importance. They are theoretically important because it has been shown that essentially the whole  $q_T$  distribution (including the low  $q_T$  region) can be predicted. The procedure for the resummation of multiple gluon emission including transverse momentum conservation was introduced in ref. (17) and further developed in refs. (18,13,19). The comparison with W boson production data at  $\sqrt{s} = 0.54$  TeV is shown in Fig. 3.

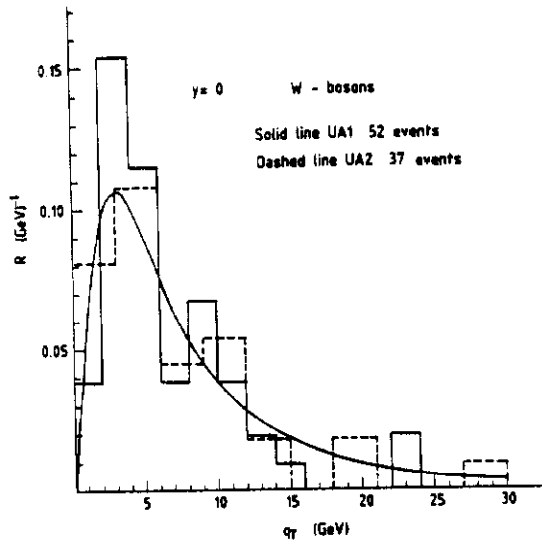


Fig. 3

The normalised differential cross-section  $R$  for the production of  $(W^+W^-)$  bosons as a function of  $q_T$  at  $\sqrt{s} = 0.54$  TeV. The dotted and dashed histograms are the suitably normalised data of the UA1 and UA2 collaborations respectively. The solid line is the theoretical prediction for

$$R = \frac{d\sigma(y=0)}{dq_T dy} / \frac{d\sigma(y=0)}{dy} \quad (20)$$

based on the parton distributions of Gluck et al.<sup>11</sup> A full analysis<sup>9</sup> of the uncertainty in the theoretical prediction due to the form of the parton distribution functions, the size of  $A$ , and the uncalculated higher order corrections shows that it is about 25%. Within the limited statistics the agreement between theory and data is acceptable. The change of the ratio  $R$  with increasing centre-of-mass energy is illustrated in Fig. 4.

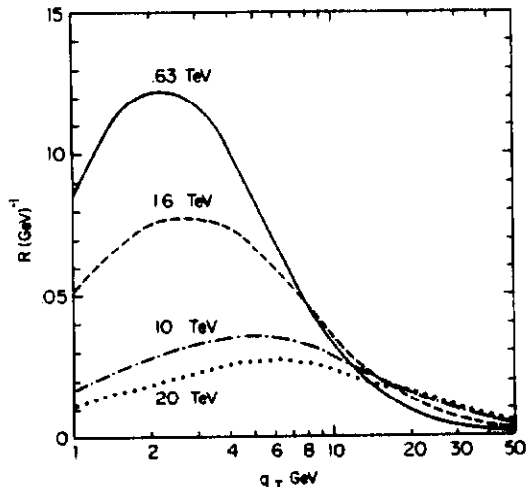


Fig. 4

The normalised differential cross-section  $R$  for the production of  $W^+W^-$  bosons in proton anti-proton collisions at various centre of mass energies.

With increasing energy a larger fraction of the events lie above  $q_T = 30$  GeV. It is therefore to this large transverse momentum tail, which is well described by the simple perturbative formula, that we turn our attention.

At super colliders the large transverse momentum region is of most interest because it is in this region that the search for physics beyond the standard model will take place.  $W$  and/or  $Z$  production at large  $q_T$  could cause "monojets" or "lepton + jet" events with missing transverse energy. Both of these types of events are typical triggers in the search for new phenomena. In order to estimate the probability of such events from conventional QCD sources, we define the quantity

$$\pi(q_T) = \int_{q_T}^{A_T} \frac{d\sigma(y=0)}{dp_T dy} dp_T / \int_0^{A_T} \frac{d\sigma(y=0)}{dp_T dy} dp_T \quad (21)$$

where  $A_T$  is the kinematic limit of the transverse momentum.

$q_T$ GeV	$\pi^W(q_T)\%$		
	$\sqrt{s}=0.54$ TeV pp	$\sqrt{s}=10$ TeV pp	$\sqrt{s}=40$ TeV pp
25	3.4 ± 0.4	---	---
30	2.0 ± 0.2	26.0	---
40	0.8 ± 0.1	16.9	---
50	0.40 ± 0.05	11.7	15.
60	0.16 ± 0.02	8.3	11.
70	---	6.0	8.
80	---	4.5	6.
90	---	3.4	5.
100	---	2.6	4.
110	---	2.1	3.
120	---	1.7	2.
130	---	1.3	2.
140	---	1.1	1.
150	---	0.9	1.

Table 2

The probability  $\pi(q_T)$  of finding a  $W$  boson above a certain  $q_T$  at various centre-of-mass energies.

In Table (2) the values of  $\pi$  at  $\sqrt{s} = 0.54$  TeV and 10 TeV for pp collisions and at  $\sqrt{s} = 40$  TeV for pp collisions are given. The results at  $\sqrt{s} = 0.54$  have been calculated using the  $O(\alpha_s^2)$  contribution<sup>20</sup> coming from quark-antiquark annihilation. The difference between  $\pi$  calculated in order  $\alpha_s$  and calculated in order  $\alpha_s^2$  is small, but inclusion of the  $O(\alpha_s^2)$  term leads to a substantial decrease in the error which is mainly due to the scale ambiguity in the running coupling constant. At the other two energies the percentage errors on  $\pi$  are of the same order as the percentage errors given in Table 1 at the corresponding energies. The figures are therefore for illustration only. Table 2 indicates that it is most unlikely to find more than 3% of the  $W$ 's (or  $Z$ 's, for which a similar result holds) with an associated jet of  $q_T \geq 35$  GeV. Taking into account the factor 6 between  $\Gamma(Z \rightarrow \nu\bar{\nu})$  and  $\Gamma(Z \rightarrow e^+e^-)$  it follows that at  $\sqrt{s} = 0.54$  TeV we should expect about five times fewer monojets with  $q_T \geq 35$  GeV, than regular  $Z$  decays to electron pairs at  $\sqrt{s} = 0.54$  TeV.

### Acknowledgements

The work described in this report was performed in collaboration with G. Altarelli and G. Martinelli.

### References

- 1) G. Altarelli. Phys. Reports 8 1, 1( 1982) and references therein.
- 2) J. C. Collins, "Theory problems at small x", these proceedings.
- 3) F. Eisele, Journal de Physique, Supplement to No.12 Volume 4 3(1982)
- 4) G. Altarelli and G. Parisi, Nucl. Phys. B126, 298(1977)
- 5) W. Furmanski and R. Petronzio, Phys. Lett. 97B 437(1980)
- 6) T. Jaroszewicz, Phys. Lett. 116B 291(1982)
- 7) D. W. Duke and J. F. Owens, Phys. Rev. D30 49(1984)
- 8) L. V. Gribov et al., Phys. Rep. 100, 1(19 83)
- 9) A. Bassetto et al., Nucl. Phys. B207 18 9(1 982)
- 10) L. N. Lipatov, Sov. J. Nucl. Phys. 23, 338(1976)
- 11) M. Gluck, E. Hoffmann and E. Reya, Z. Phys. C13 119(1982)
- 12) E. Eichten, I. Hinchliffe, K. Lane, and C. Quigg, Rev. Mod. Phys. 56 (1984)
- 13) G. Altarelli, R. K. Ellis, M. Greco and G. Martinelli, Nucl. Phys. B246 12(1984)
- 14) G. Altarelli, R. K. Ellis and G. Martinelli, Nucl. Phys. B157 461(1979)  
J. Kubar-Andre and F. E. Paige, Phys. Rev. D19 221(1979)
- 15) UA1 Collaboration, G. Arnison et al., Phys. Lett. 139B 115 (1984)
- 16) UA2 Collaboration, P. Bagnaia et al., Phys. Lett. 139B 105 (1984)
- 17) G. Parisi and R. Petronzio, Nucl. Phys. B17674 427(1979) G. Curci, M. Greco and Y. Srivastava, Phys. Rev. Lett. 43 434(1979) Nucl. Phys. B159 451(1979)
- 18) S.-C. Chao and D. E. Soper, Nucl. Phys. B124 405(1983) S.-C. Chao, D. E. Soper and J. C. Collins, Nucl. Phys. B214 513(1983)
- 19) C. T. H. Davies and W. J. Stirling, Nucl. Phys. B244 337 (1984) references therein.
- 20) R. K. Ellis, G. Martinelli and R. Petronzio, Nucl. Phys. B211 106(1983)
- 21) G. Altarelli, R. K. Ellis and G. Martinelli, CERN preprint TH 4015 (1984)